Chalcogenide Letters Vol. 21, No.8, August 2024, p. 631 - 640

Vacancy-defect promoting blue LED-driven H_2O_2 synthesis on $Zn_{0.4}Cd_{0.6}S$ without additional cocatalysts

W. W Lu, J. N. Ding, Z. Y. Wang, Y. C Wei, Y. P. Chen, J. Xu*
School of Physics and Electronic Engineering, Jingjiang College, Jiangsu University, Zhenjiang, China, 212013, P. R.
Quantum Sensing and Agricultural Intelligence Detection Engineering Center of Jiangsu Province, Zhenjiang, Jiangsu, 212013, P. R. China

Photocatalytic synthesis of hydrogen peroxide offers an effective solution to the energy crisis. The design and development of high-activity and low-cost photocatalysts are crucial for H_2O_2 production. In this work, $Zn_{0.4}Cd_{0.6}S$ with abundant S vacancies (S_V-ZCS) is developed for H_2O_2 photosynthesis under 405 nm LED illumination without additional cocatalysts. The S vacancies serve as photo-generated electron trap centers, effectively extending the lifetimes of photogenerated carriers and promoting the separation of photoelectric carriers. Additionally, S_V-ZCS is endowed with enhanced light capture capability, enhancing the overall photocatalytic activity for H_2O_2 production. The results were in line with expectations, the S_V-ZCS samples demonstrated a hydrogen peroxide (H_2O_2) productivity of 3902 μmol L^{-1} h^{-1} when subjected to visible light irradiation, representing a significant increase compared to that of ZCS (2840 μmol L^{-1} h^{-1}). This work provides an effective strategy for preparing photocatalysts for efficient hydrogen peroxide production.

(Received May 25, 2024; August 12, 2024)

Keywords: S vacancies, Zinc cadmium sulfide, Hydrogen peroxide production, Photocatalysis

1. Introduction

Hydrogen peroxide (H_2O_2) is an essential multifunctional chemical resource, that is employed in a multitude of applications, including pulp bleaching, wastewater treatment, medical disinfection, organic synthesis, and others [1,2,3]. Currently, the industrial production of H_2O_2 relies heavily on the energy-intensive anthraquinone process, where 2-alkyl tetraquinone is hydrogenated by a costly palladium catalyst. Hydrogenation of hydrogen peroxide by an expensive palladium catalyst is an unsatisfactory process in terms of energy saving and cost [4,5]. Consequently, one of the most promising research avenues is the development of green and efficient production methods for hydrogen peroxide [6,7].

Photocatalysis has emerged as a promising green technology that reduces our dependence on unsustainable fossil fuels and minimizes environmental pollution. Current research focuses on key photocatalytic reactions including hydrogen production by water decomposition [8,9,10], CO_2 reduction [11,12], CH_4 oxidation, degradation of organic compounds [13], N_2 photofixation [14], and H_2O_2 synthesis. Photocatalytic production of H_2O_2 typically occurs on semiconductors. Upon absorption of light, when photons with energy exceeding the band gap of semiconductors are present, electrons are excited from the valence band (VB) to the conduction band (CB) of semiconductors. The resulting photogenerated electrons (e^-) and holes (h^+) either combine again or move toward the surface of the photocatalyst for a redox reaction [15,16,17], in which H_2O_2 is formed by the e^- reducing O_2 or the h^+ oxidizing water. In comparison to the conventional method of H_2O_2 production, the photocatalytic approach offers several distinctive advantages. Firstly, it is economically efficient and conserves energy by utilizing abundant water and/or gaseous O_2 as raw materials along with

* Corresponding author: xjing@ujs.edu.cn
https://doi.org/10.15251/CL.2024.218.631

solar energy as its sole power source. Secondly, this method is environmentally friendly due to water (H_2O, H^+ , and OH^-) being the only by-product. Overall, photocatalysis holds significant promise for sustainable technological advancement through its effective resource utilization and minimal environmental impact.

However, current photocatalytic production of H_2O_2 often has some shortcomings, such as low carrier separation and transmission efficiency, poor light absorption capacity, and few active sites [18,19,20]. Among all types of existing photocatalysts, metal sulfides, notably CdS and ZnS, have garnered significant attention owing to their inherent optical and electronic properties. CdS has a narrow bandwidth, suitable CB and VB positions, and wide absorption in the visible range. Furthermore, thermal treatment is more likely to facilitate the development of a closely integrated interface between CdS and the auxiliary catalyst, which is crucial for determining the photocatalytic performance of water decomposition [21]. Additionally, owing to the high position of ZnS in the conductive band, it could be used in the photocatalytic decomposition of water into a sacrificial solution for the analysis of hydrogen without the need for precious metal catalysis. A study by Reber et al. in 1984 showed that Ag_2S could enhance the photocatalytic activity of CdS powders and that ZnS doping could further improve catalytic performance [22]. $Zn_XCd_{1-X}S$ is a solid solution combining the advantages of CdS and ZnS [23]. It features an adjustable bandgap and edge position, a facile synthesis process, a robust response to visible light irradiation, as well as high photostability. The absorption edge of $Zn_XCd_{1-X}S$ is between ZnS and CdS, and the Zn/Cd ratio during the preparation process affects the change in its bandwidth and belt edge position.

In this work, $Zn_XCd_{1-X}S$ was selected as the starting point, with x=0.4. This was then subjected to defect engineering to explore the generation of photocatalytic hydrogen peroxide. As a result, S_V-$Zn_{0.4}Cd_{0.6}S$ material (S_V-ZCS) was prepared, which was rich in S vacancies. When lactic acid was employed as a sacrificial agent and the balloon was continuously filled with oxygen, the yield of hydrogen peroxide was as high as 7804.7 μmol L^{-1} at 2 hours, representing an approximately 12-fold increase compared to experiments conducted without a sacrificial agent present. In comparison with the pure sample (ZCS) under identical conditions, this result has also been significantly enhanced. The findings of this study may pique the interest of a broader audience in the field of photocatalysis, offering novel insights into the synthesis of catalyst materials.

2. Experimental section

2.1. Experimental chemicals

The materials utilized in this experiment included cadmium acetate dihydrate ($Cd(CH_3COO)_2{\cdot}2H_2O$, ≥99.9%), zinc acetate dihydrate ($Zn(CH_3COO)_2{\cdot}2H_2O$, ≥99.0%), and ethylenediamine. ($C_2H_8N_2$, ≥99.0%), Thioacetamide (TAA, C_2H_5NS, ≥99.0%), Hydrazine hydrate aqueous solution ($N_2H_4{\cdot}H_2O$, ≥85.0%). All experiments were conducted using ultrapure water. The aforementioned chemicals were procured from commercial sources without undergoing additional purification processes.

2.2. Preparation of $Zn_{0.4}Cd_{0.6}S$ (ZCS)

To experiment, 4 mmol of $Zn(CH_3COO)_2{\cdot}2H_2O$ should be dissolved in a solution consisting of $C_2H_8N_2$ and deionized water (25 mL water and 25 mL $C_2H_8N_2$), followed by the addition of 6 mmol of $Cd(CH_3COO)_2{\cdot}2H_2O$. Upon clarification of the solution, 13 mmol TAA should be introduced, with stirring for 30 minutes. Subsequently, the resulting mixture is to be transferred into a 50 mL reactor and subjected to a reaction at a temperature of 220 °C for 24 hours. Following cooling of the reactor to room temperature, it must undergo centrifugation at a rate of 9000 r min^{-1} for 5 minutes before undergoing multiple washes with deionized water and anhydrous ethanol. The resultant sediment is then to be placed within a vacuum drying box set at a temperature of 60 °C for an overall duration totaling up to 12 hours to yield the final sample comprising the $Zn_{0.4}Cd_{0.6}S$ solid solution.

2.3. Preparation of S_V-$Zn_{0.4}Cd_{0.6}S$ (SV-ZCS)

Disperse the synthetic 100 mg $Zn_{0.4}Cd_{0.6}S$ in 20 ml deionized water for one hour. Subsequently, add 5 ml of $N_2H_4 \cdot H_2O$ to the mixed solution and stir for another 30 minutes. Then transfer the mixture to a 50 mL stainless steel still and keep it at 240°C for 5 hours. The pellet was then isolated through centrifugation and subjected to multiple rinses with demineralized water. Finally, the powder was subjected to drying at a temperature of 60 °C for 10 hours, resulting in the light-yellow powder, which was labelled as S_V-$Zn_{0.4}Cd_{0.6}S$.

2.4. Characterizations

The sample was analyzed via X-ray diffraction (XRD) using an X-ray diffraction apparatus (Bruker D_2 Phaser) and Cu Kα radiation (λ = 1.5418 Å) at an operating voltage of 40 kV. SEM examinations were conducted utilizing a field-emitting scanning electron microscope (JSM-7001F). TEM images and EDS mapping were captured employing a Thermo Fisher Scientific microscope (JEM-2100). X-ray photoelectron spectroscopy (XPS) analysis was conducted with Al-Kα radiation using a K Alpha instrument manufactured by Thermo Scientific. Diffuse ultraviolet reflectance spectra (DRS) analysis was conducted on the prepared samples using a UV-Vis spectrometer (UV2550, Shimadzu, Japan). Photoluminescence (PL) assessments were carried out using a JASCO FP-6500 fluorescence spectrophotometer. The luminescence lifetime was determined via a single photon counting spectrometer featuring a source with an excitation wavelength of 380 nm. All photoelectrochemical properties were comprehensively assessed using the potentiostat (CHI660B), which included the analysis of transient photocurrent response and electrochemical impedance spectroscopy (EIS). Throughout the evaluation, a conventional system featuring three electrodes was employed, including a platinum plate as a counter electrode and $Hg/Hg_2Cl_2/Cl$ as a reference electrode, in a 0.1 M Na_2SO_4 solution.

2.5. Photocatalytic H_2O_2 production

The synthesis of H_2O_2 using photocatalysis was conducted within a sophisticated photochemical multichannel reaction system. To initiate the process, 10 mg of catalyst was carefully dispersed in a Shi Ying three-necked flask, which held 45 ml of deionized water and 5 ml of sacrificial agent. The flask was then securely sealed with a rubber membrane cover. Utilizing ultrasonication and stirring, the catalyst was meticulously dispersed until it achieved uniform dissolution in the solution. After stirring for 15 minutes, the flask was aerated with O_2 for 15 minutes. Fill the flask with a balloon filled with O_2, and take the first sample for 0 minutes with a disposable syringe. The LED lamp with a wavelength of 420nm was used to illuminate the photocatalyst suspension from the front. Samples were taken every 20 minutes and 1 mL of the sample was collected from the suspension. The collected solution was filtered with a syringe filter (0.22 microns) to remove the photocatalyst. The total illumination time was 2 hours. The amount of H_2O_2 production was determined by iodometry. Take 50 microliters from the corresponding samples at each time, add 0.5 ml of 0.1 mol of potassium hydrogen phthalate ($C_8H_5KO_4$) and 0.5 ml of 0.4 mol of potassium iodide (KI) respectively, and wait 30 minutes for complete color development. Under acidic conditions ($H_2O_2 + 3I^- + 2H^+ \rightarrow I_3^- + 2H_2O$), H_2O_2 reacted with the iodide anion (I^-) to form a triiodide anion (I_3^-), which has a strong absorbance at about 350 nm. Utilizing UV-Vis spectroscopy, the quantity of I^{3-} was determined based on its absorbance at this wavelength, thereby enabling estimation of the amount of H_2O_2 produced in each reaction phase.

3. Results and discussion

3.1. Characterizations of the samples

$Zn_{0.4}Cd_{0.6}S$ (ZCS) nanoparticles were synthesized utilizing $Zn(CH_3COO)_2 \cdot 2H_2O$, $Cd(CH_3COO)_2 \cdot 2H_2O$, and thioacetamide (TAA) as precursor materials. The creation of S_V-ZCS, featuring S vacancies within the ZCS structure, was achieved through the thermal treatment of ZCS in an oxygen-rich environment at 240°C for 5 hours (Fig. 1a). The morphological and structural attributes of this photocatalyst were thoroughly examined using cutting-edge techniques including

scanning electron microscopy (SEM), transmission electron microscopy (TEM), and aberration-corrected transmission electron microscopy (AC-TEM). SEM images (Fig. 1b) and TEM images (Fig. 1c) showed that S_V-$Zn_{0.4}Cd_{0.6}S$ (S_V-ZCS) consists of irregular particles. A more detailed analysis of the high-resolution TEM (HRTEM) images of these nanoparticles was presented in Fig. 1d and Fig. 1e. The fuzzy fringes of the network in the yellow region indicated the numerous surface defects in the S_V-ZCS (Fig. 1d) [24]. Additionally, an ordered lattice fringe with a spacing of 0.36 nm corresponding to the facet (002) planes was observed in Fig. 1e [25]. In addition, Fig. 1f shows the mapping of the EDS elements for S_V-ZCS-based TEM. It was evident that the Zn, Cd, and S elements had a uniform distribution, consistent with the microscopic morphology, rather than an obvious lack of these elements in a particular region. This indicated a uniform distribution of these surface defects. The XRD results (Fig. 1g) showed that the diffraction peaks of $Zn_{0.4}Cd_{0.6}S$ corresponded to the diffraction peaks of hexagonal $Zn_{0.2}Cd_{0.8}S$ (JCPDS card No. 49-1302). It was noteworthy that the S_V-ZCS sample exhibited an XRD pattern almost identical to that of ZCS, suggesting that the introduction of S vacancies had minimal impact on the size and crystal structure of ZCS [26].

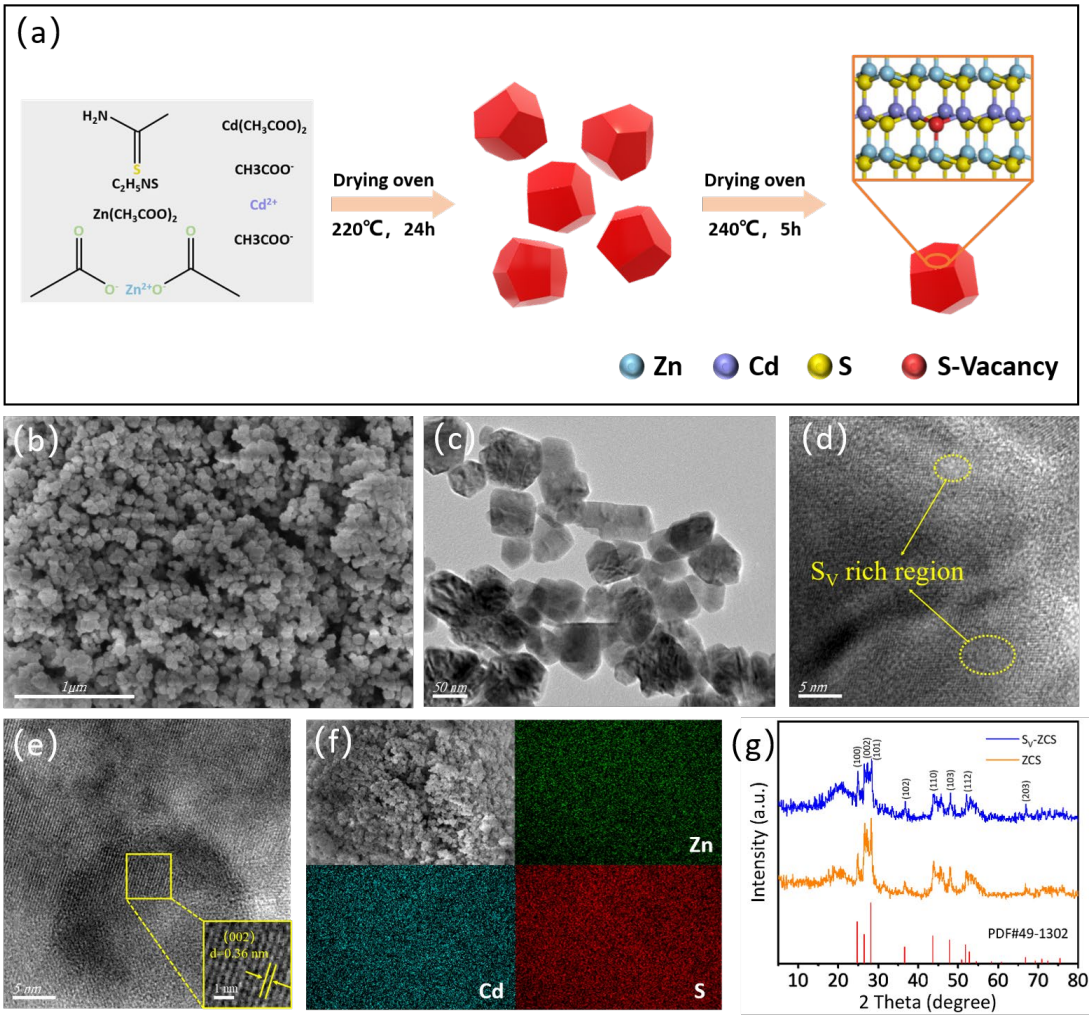

Fig. 1. Characterizations of S_V-ZCS. (a) Representation of the formation. (b) SEM image of S_V-ZCS. (c) TEM image of S_V-ZCS. (d, e) HRTEM images of S_V-ZCS. (f) SEM mapping images of S_V-ZCS. (g) XRD patterns of S_V-ZCS and ZCS.

3.2. Evaluation of photocatalytic performance

Given the facilitation of low-coordinated centers in adsorbing H_2O, it was hypothesized that S_V-ZCS could function as a promising photocatalyst for synthesizing H_2O_2 from H_2O and O_2. It was

observed that the formation of S_V in ZCS could enhance light absorption (Fig. 2a). Additionally, it was observed that there existed a positive correlation between the band gaps and the presence of S_V (Fig. 2b) [27]. In this study, ZCS and S_V-ZCS were employed as photocatalysts to drive the reduction of O_2 and the oxidation of H_2O to produce H_2O_2 under visible-light irradiation. In addition, to produce more hydrogen peroxide, we added sacrifice agents. As depicted in Fig. 2c, S_V-ZCS acted as a substrate while lactic acid, ethanol, and ethylene glycol, among others, were employed as sacrificial agents for catalyzing hydrogen peroxide production. The utilization of lactic acid resulted in a remarkable increase in hydrogen peroxide concentration reaching 7804.7 μmol L^{-1} at 2 h, surpassing non-sacrificial agents by 12-fold (640.5 μmol L^{-1}). The hydrogen peroxide productivity of S_V-ZCS was more than 2000 μmol L^{-1} than ZCS (5681.1 μmol L^{-1}) at 2 h under lactic acid sacrifice (Fig. 2d).

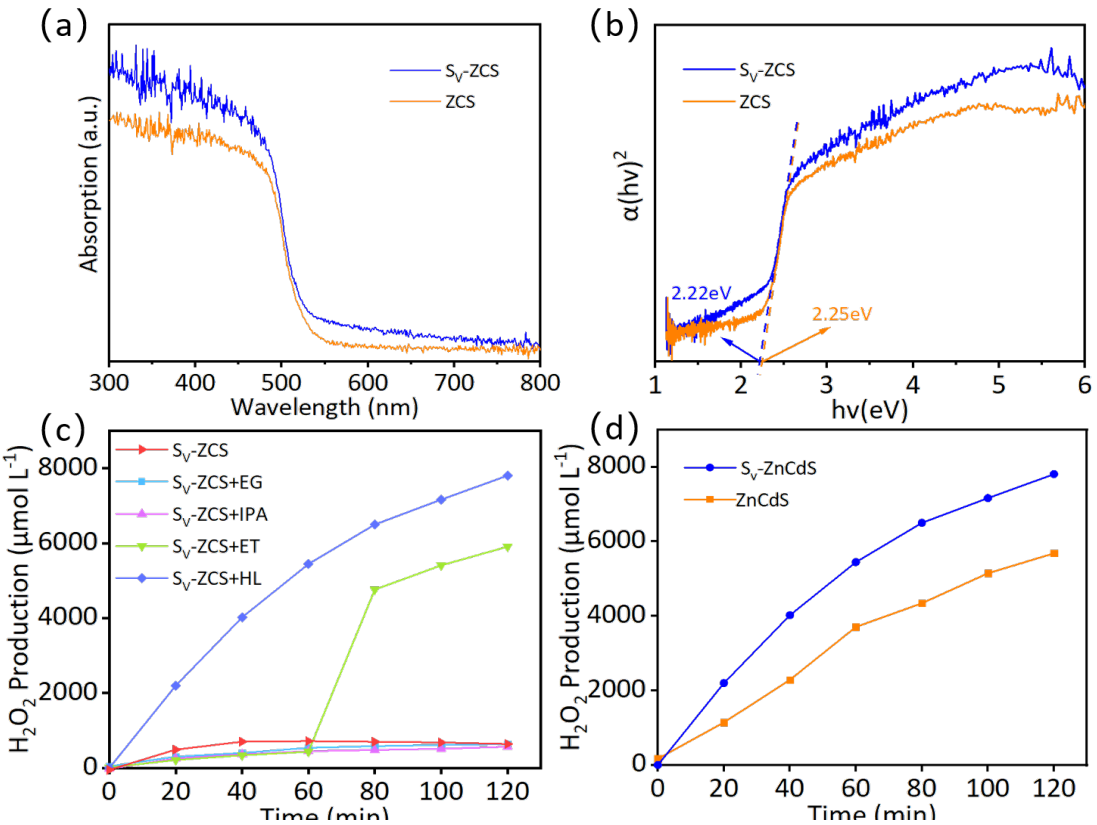

Fig. 2. Photocatalytic performance of S_V-ZCS. (a) UV-Vis diffuse reflectance spectra of the as-prepared S_V-ZCS and ZCS. (b) Tauc plots of S_V-ZCS and ZCS samples. (c) Time-dependent photocatalytic H_2O_2 production for S_V-ZCS under different sacrifice agents. (d) Time-dependent photocatalytic H_2O_2 production for S_V-ZCS and ZCS under lactic acid sacrifice.

3.3. Mechanism investigations

To elucidate the underlying reasons for the enhanced photocatalytic properties resulting from the incorporation of S_V, steady-state photoluminescence spectroscopy (PL) was utilized to evaluate the separation of the photogenerated electrons and holes. The PL emission intensity of S_V-ZCS was slightly lower than that of ZCS (Fig. 3a), indicating that the presence of S vacancies had a slight inhibitory effect on the recombination of photogenerated electron-hole pairs [28]. The temporal attenuation kinetics of time-resolved photoluminescence (TPRL) spectral attenuation of the prepared ZCS were adjusted using a three-exponential model (Fig. 3b). The results showed that S_V-ZCS had a shorter mean emission duration than ZCS (1.95 ns), indicating that the presence of S_V could effectively enhance the photoexciton transfer to the electron acceptors [29]. Subsequent

investigation into the mechanism of efficient charge separation and transfer in S_V-ZCS catalyst was accomplished through surface photovoltage spectroscopy (SPV). For the S_V-ZCS catalyst, a significant increase in surface tension was observed, indicating an improved efficiency of charge transfer (Fig. 3c). In addition, the photoelectrochemical properties were investigated to demonstrate the best photocatalytic performance of S_V-ZCS. As illustrated in Fig. 3d, the introduction of S_V led to a significant increase in current density for ZCS, suggestive of enhanced separation and transformation efficiency of photogenerated electron-hole pairs in S_V-ZCS [30]. Compared to the electrochemical impedance spectrum (EIS) of pure ZCS without S_V, the smaller semicircle radius indicated that S_V formation could reduce the charge transfer resistance and facilitate the separation of photogenerated charge carriers (Fig. 3e) [31]. In addition, our investigation into electrochemical hydrogen peroxide production confirmed elevated performance levels achieved by utilizing electrodes comprised with S_V-ZCS through the employment of linear scanning voltammetry technique (Fig. 3f).

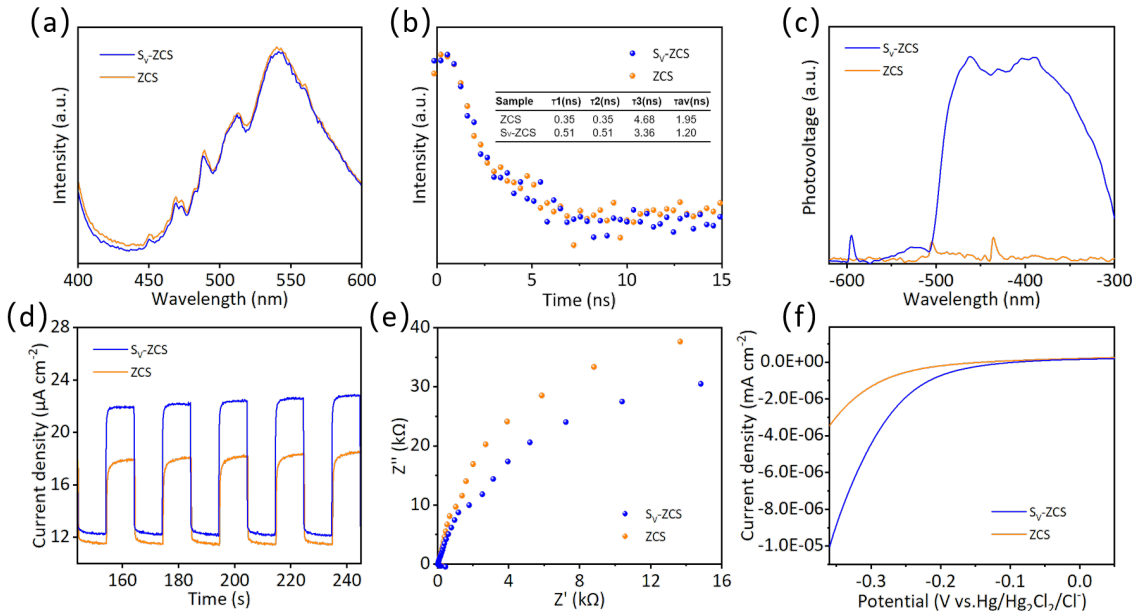

Fig. 3. (a) Steady-state photoluminescence spectra. (b) Time-resolution PL spectra. (c) Surface photovoltage method (SPV). (d) Transient photocurrent spectra. (e) Electrochemical impedance spectroscopy spectra (EIS) and (f) Linear sweep voltammetry (LSV) of S_V-ZCS and ZCS samples.

To further elucidate the mechanism behind hydrogen peroxide production in S_V-ZCS, the VB energy, and CB energy were calculated to determine the band position of ZCS and S_V-ZCS. Formula (1) was employed in conjunction with the VB-XPS energy (Fig. 4a, 4b) to calculate the VB-NHE energy.

$$E_{VB,NHE} = \varphi + E_{VB,XPS} - 4.44 \quad (1)$$

where φ represents the intrinsic work function of the X-ray photoelectron spectroscopy (XPS) instrument, measuring at an energy level of 4.6 electron volts (eV). As a result, it can be calculated that the valence band (VB) energy levels of both ZCS and S_V-ZCS are 0.88 eV and 0.79 eV, respectively. By combining these values with the band gap width obtained from ultraviolet spectroscopy, the band positions of the samples can be determined using formula (2) as shown in Figure 4c.

$$E_g = E_{VB} - E_{CB} \quad (2)$$

Based on the empirical evidence and analytical findings presented above, the schematic representation of the mechanism for enhancing the photocatalytic generation of hydrogen peroxide by S_V-ZCS is illustrated in Fig. 4d. First, due to the irregular structure of the nanoparticles, ZCS provided an optimal optical transport pathway to guide the light energy within the ZCS, absorbing more visible light and creating carriers with more electron gaps [32]. In addition, a large number of S-vacancies introduced a new level of donors into the ZCS band gap, resulting in a reduction in band gap energy and improved utilization of visible light. Furthermore, photoelectrons produced from optical transitions between conduction bands and valence bands are effectively captured at empty S sites due to their alignment with defect levels and conduction bands under sunlight [33]. This also promoted the oxygen reduction reaction in the S-vacancy, which had excellent chemical activity. Consequently, surface vacancies acted as effective capture sites for photoelectrons while also promoting electron transfer kinetics and accelerating consumption rates. These processes ultimately contribute to enhanced photocatalytic production of hydrogen peroxide by supporting efficient separation and transfer mechanisms for photogenerated electron-hole pairs [34,35]. Simultaneously, the absorption of sacrificial agents (HL) present in solution results in continuous consumption of photogenerated holes generating H_2O and CO_2 which further facilitates separation and transfer processes within S_V-ZCS. Furthermore, the inhibition of charge recombination increased the photocatalytic activity of S_V-ZCS against hydrogen peroxide. The increase in CB after the formation of the S-defect further enhanced the reduction capacity of the photoelectrons and accelerated the reduction reaction at the surface [36]. These factors together contributed to the observation of increased catalytic activity of S-deficient ZCS in hydrogen peroxide production. As a result, the reaction pathway of H_2O_2 photosynthesis was summarized as follows (Fig. 4e). S_V in S_V-ZCS could facilitate the separation of electrons and holes generated by light.

$$S_V - ZCS + hv \rightarrow h^+ + e^-$$

The electron reacted with O_2 and produced $\bullet O_2^-$.

$$O_2 + e^- \rightarrow \cdot O_2^-$$

The last reaction was the formation of H_2O_2 by the reaction of $\bullet O_2^-$ and H^+.

$$O_2^- + 2H^+ + e^- \rightarrow H_2O_2$$

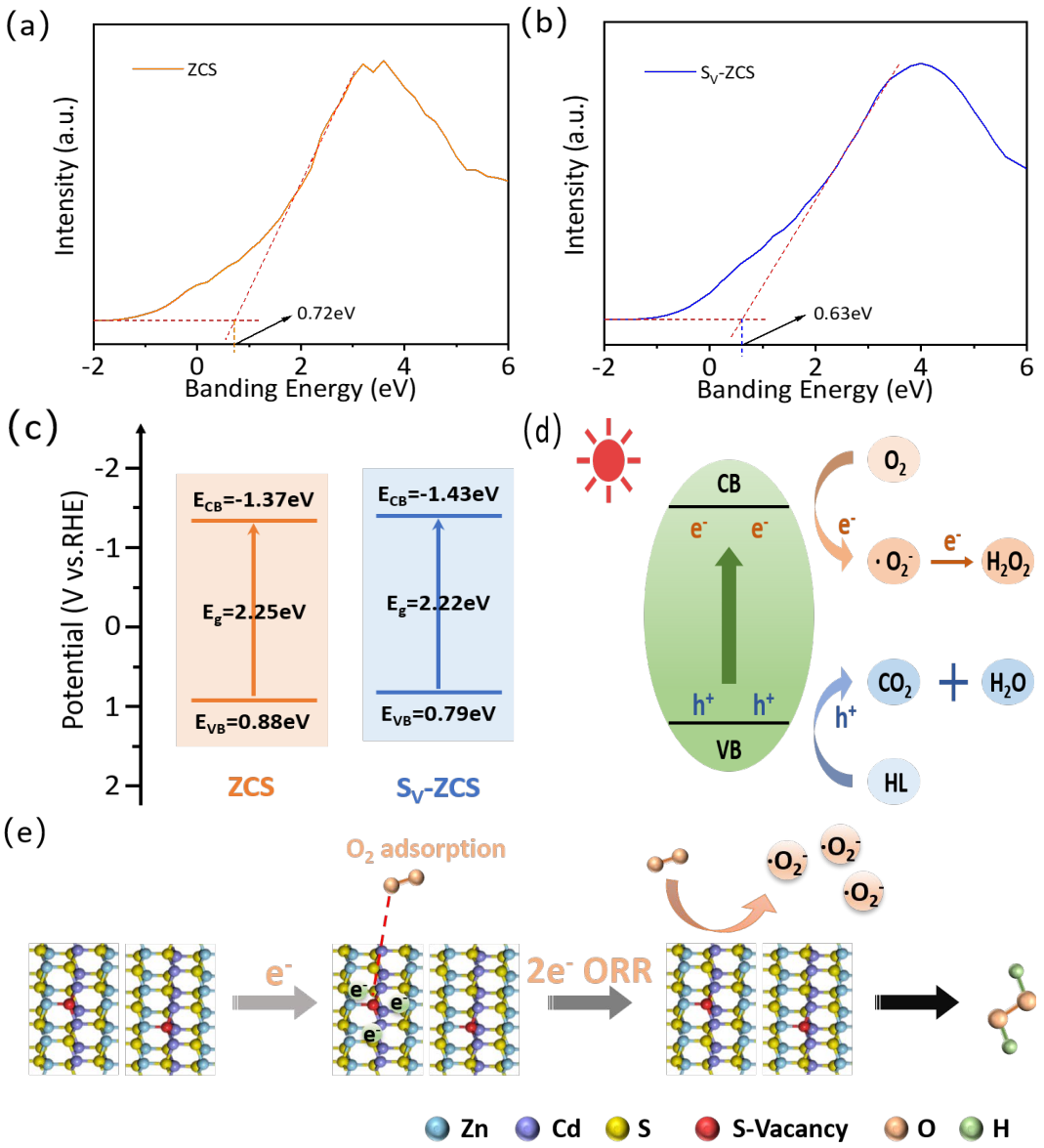

Fig. 4. (a) VB-XPS for ZCS. (b) VB-XPS for S_V-ZCS. (c) Band structures of ZCS and S_V-ZCS. (d) Photocatalytic H_2O_2 production process involving. (e) Scheme for H_2O_2 photosynthesis over S_V-ZCS.

4. Conclusions

In summary, in this work, Sv-$Zn_{0.4}Cd_{0.6}S$ (S_V-ZCS) nanoparticle photocatalyst material rich in S vacancies was prepared using $Zn_{0.4}Cd_{0.6}S$ as a precursor, which could be used for the photocatalytic synthesis of H_2O_2 by oxygen reduction under lactic acid as a sacrificial agent. A series of detailed characterizations and experimental data showed that S_V-ZCS exhibited better charge separation and transfer efficiency by introducing S-vacancies, enriched the total active sites of the photocatalytic reaction, and improved the light absorption capacity of the precursor materials without changing the light absorption range. These improvements have significantly improved the overall photocatalytic activity of H_2O_2 production. S_V-ZCS was the best catalyst. When exposed to visible light, the yield of H_2O_2 was 7804.7 μmol L^{-1} at 2 hours. Compared to ZCS (5681.1 μmol L^{-1}), it was about 2000 μmol L^{-1} higher than most photocatalysts reported so far under the same conditions. The results of this work may arouse the interest of more people in the field of photocatalysis and provide an effective strategy for preparing photocatalysts that could efficiently produce hydrogen peroxide.

Acknowledgments

This research was supported by the National Natural Science Foundation of China (22302079), and the Natural Science Foundation of Jiangsu Province (BK20230521).

References

[1] E. Jung, H. Shin, B. H. Lee, V. Efremov, S. Lee, H. S. Lee, J. Kim, W. Hooch Antink, S. Park, K. S. Lee, S. P. Cho, J. S. Yoo, Y. E. Sung, T. Hyeon, Nature Materials 19, 436-442 (2020); https://doi.org/10.1038/s41563-019-0571-5
[2] Z. Tian, C. Han, Y. Zhao, W. Dai, X. Lian, Y. Wang, Y. Zheng, Y. Shi, X. Pan, Z. Huang, H. Li, W. Chen, Nature Communications 12, 2039 (2021); https://doi.org/10.1038/s41467-021-22394-8
[3] J. K. Lee, H. S. Han, S. Chaikasetsin, D. P. Marron, R. M. Waymouth, F. B. Prinz, R. N. Zare, Proceedings of the National Academy of Sciences of the United States of America 117(49), 30934-30941 (2020); https://doi.org/10.1073/pnas.2020158117
[4] J. J. Gao, H. B. Yang, X. Huang, S. F. Hung, W. Z. Cai, C. M. Jia, S. Miao, H. M. Chen, X. F. Yang, Y. Q. Huang, T. Zhang, B. Liu, Chem 6, 658 (2020); https://doi.org/10.1016/j.chempr.2019.12.008
[5] Y. Wang, G. I. N. Waterhouse, L. Shang, T. R. Zhang, Advanced Energy Materials 11, 2003323 (2020); https://doi.org/10.1002/aenm.202003323
[6] Z. Y. Teng, Q. Zhang, H. B. Yang, K. Kato, W. Yang, Y. R. Lu, S. Liu, C. Wang, A. Yamakata, C. L. Su, B. Liu, T. Ohno, Nature Catalysis 4, 374-384 (2021); https://doi.org/10.1038/s41929-021-00605-1
[7] L. Chen, C. Chen, Z. Yang, S. Li, C. H. Chu, B. L. Chen, Advanced Functional Materials 31, 2105731 (2021); https://doi.org/10.1002/adfm.202105731
[8] J. Bai, W. Chen, R. Shen, Z. Jiang, P. Zhang, W. Liu, X. Li, Journal of Materials Science & Technology 112, 85-95 (2022); https://doi.org/10.1016/j.jmst.2021.11.003
[9] R. C. Shen, C. C. Qin, L. Hao, X. Z. Li, P. Zhang, X. Li, Advanced Materials 35, 2305397 (2023); https://doi.org/10.1002/adma.202305397
[10] M. Li, M. Van Der Veer, X. Yang, B. Weng, L. Shen, H. Huang, X. Dong, G. Wang, M. B. J. Roeffaers, M. Yang, Journal of Colloid and Interface Science, 657, 819-829 (2024); https://doi.org/10.1016/j.jcis.2023.11.171
[11] K. He, R. Shen, L. Hao, Y. Li, P. Zhang, J. Jiang, X. Li, Acta Phys. -Chim. Sin. 38 (11), 2201021 (2022); https://doi.org/10.3866/PKU.WHXB202201021
[12] Y. Xia, B. Cheng, J. Fan, J. Yu, G. Liu, Science China Materials 63, 552-565 (2020); https://doi.org/10.1007/s40843-019-1234-x
[13] T. Tasso Guaraldo, J. Wenk, D. Mattia, Advanced Sustainable Systems 5, 2000208 (2021); https://doi.org/10.1002/adsu.202000208
[14] Z. Wang, J. Hong, S.-F. Ng, W. Liu, J. Huang, P. Chen, W.-J. Ong, Acta Physico-Chimica Sinica 37, 2011033 (2020); https://www.whxb.pku.edu.cn/EN/10.3866/PKU.WHXB202011033
[15] K. H. Huang, J. X. Bai, R. C. Shen, X. Z. Li, C. C. Qin, P. Zhang, X. Li, Advanced Functional Materials 33, 2307300 (2023); https://doi.org/10.1002/adfm.202307300
[16] M. C. Liu, P. Ye, M. Wang, L. L. Wang, C. Wu, J. Xu, Y. P. Chen, Journal of Environmental Chemical Engineering 10, 108436 (2022); https://doi.org/10.1016/j.jece.2022.108436
[17] R. C. Shen, N. Li, C. C. Qin, X. Z. Li, P. Zhang, X. Li, J. W. Tang, Advanced Functional Materials 33, 2301463 (2023); https://doi.org/10.1002/adfm.202301463
[18] L. L. Wang, Y. Hu, J. H. Xu, Z. F. Huang, H. X. Lao, X. W. Xu, J. Xu, H. Tang, R. S. Yuan, Z. Wang, Q. Q. Liu, International Journal of Hydrogen Energy 48 (45), 16987-16999 (2023); https://doi.org/10.1016/j.ijhydene.2023.01.172
[19] L. L. Wang, G. G. Tang, S. Liu, H. L. Dong, Q. Q. Liu, J. F. Sun, H. Tang, Chemical Engineering Journal 428, 131338 (2022); https://doi.org/10.1016/j.cej.2021.131338
[20] R. C. Shen, G. J. Liang, L. Hao, P. Zhang, X. Li, Advanced Materials 35, 2303649 (2023); https://doi.org/10.1002/adma.202303649
[21] J. F. Reber, M. Rusek, The Journal of Physical Chemistry 90, 824-834 (1986);

https://doi.org/10.1021/j100277a024
[22] W. Zhong, X. Huang, Y. Xu, H. Yu, Nanoscale 10, 19418-19426 (2018); https://doi.org/10.1039/C8NR06883F
[23] W.-H. Huang, X.-M. Li, X.-F. Yang, X.-X. Zhang, H.-H. Wang, H. Wang, Materials Chemistry Frontiers 5, 3593-3613 (2021); https://doi.org/10.1039/D0QM00936A
[24] J. Xu, P. Ye, Y. Cheng, L. Ji, Y. Wei, Y. Chen, Energy Technology, 11, 2201452 (2023); http://doi.org/10.1002/ente.202201452
[25] L. Y. Long, G. Y. Lv, F. Pan, Z. Y. Li, H. M. Zhu, D. H. Wang, Chem. C 127 (50), 24077-24087 (2023); https://doi.org/10.1021/acs.jpcc.3c07314
[26] L. M. Duan, X. D. Li, Y. M. Shang, Y. H. Feng, H. H. Fan, S. Q. Wang, B. Yang, Digest Journal of Nanomaterials and Biostructures 19(1), 369-382 (2024); https://doi.org/10.15251/DJNB.2024.191.369
[27] Q. H. Zhu, Z. H. Xu, Q. Y. Yi, M. Nasir, M. Xing, B. Qiu, J. Zhang, Materials Chemistry Frontiers 4, 3234-3239 (2020); https://doi.org/10.1039/D0QM00464B
[28] L. L. Wang, R. J. Sa, Y. C. Wei, X. F. Ma, C. G. Lu, H. W. Huang, E. Fron, M. Liu, W. Wang, S. P. Huang, J. Hofkens, MBJ. Roeffaers, Y. J. Wang, J. H. Wang, J. L. Long, X. Z. Fu, R. S. Yuan, Angewandte Chemie International Edition 61(39), 4561 (2022); https://doi.org/10.1002/anie.202204561
[29] Y. C. Wei, W. Y. Zha, L. L. Wang, X. F. Ma, S. H. Zhang, R. J. Sa, H. X. Lin, Z. X. Ding, J. L. Long, X. Z. Fu, R. S. Yuan, Applied Catalysis B: Environmental 306, 121103 (2022); https://doi.org/10.1016/j.apcatb.2022.121103
[30] J. C. Solis Cortazar, A. K. López Matus, L. Rojas Blanco, G. Pérez Hernández, I. Zamudio Torres, B. L. Pérez Escobar, R. Castillo Palomera, E. Ramírez Morales, Digest Journal of Nanomaterials and Biostructures 19(2), 493-502 (2024); https://doi.org/10.15251/DJNB.2024.192.493
[31] L. F. Yang, Y. H. Wang, Y. Peng, Nanoscale 16, 5267-5279 (2024); https://doi.org/10.1039/d3nr06419k
[32] X. Li, J. G. Yu, J. X. Low, Y. P. Fang, J. Xiao, X. B. Chen, J. Mater. Chem. A 3, 2485-2534 (2015); https://doi.org/10.1039/C4TA04461D
[33] L. L. Wang, T. Yang, L. J. Peng, Q. Q. Zhang, X. L. She, H. Tang, Q. Q. Liu, Chinese Journal of Catalysis 43(10), 2720-2731 (2022); https://doi.org/10.1016/S1872-2067(22)64133-0
[34] R. C. Shen, X. Z. Li, C. C. Qin, P. Zhang, X. Li, Advanced Energy Materials 13 (13), 2203695 (2023); https://doi.org/10.1002/aenm.202203695
[35] H. Huang, J. Zhao, H. Guo, B. Weng, H. Zhang, R. A. Saha, M. Zhang, F. Lai, Y. Zhou, R. Juan, P. Chen, S. Wang, J. A. Steele, F. Zhong, T. Liu, J. Hofkens, Y. Zheng, J. Long, M. B. J. Roeffaers, Advanced Materials 2313209 (2024); https://doi.org/10.1002/adma.202313209
[36] J. Gao, Z. Lu, C. Jin, X. Yu, H. Jiang, L. Wang, L. Sun, W. Wang, Q. Liu, Fuel, 333, 126331 (2023); https://doi.org/10.1016/j.fuel.2022.126331